

The Effect of Complex Dispersion and Characteristic Impedance on the Gain of Superconducting Traveling-Wave Kinetic Inductance Parametric Amplifiers

Javier Carrasco , Daniel Valenzuela , Claudio Falcón, Ricardo Finger, and Fausto Patricio Mena 

Abstract—Superconducting traveling-wave parametric amplifiers are a promising amplification technology suitable for applications in submillimeter astronomy. Their implementation relies on the use of Floquet transmission lines in order to create strong stopbands to suppress undesired harmonics. In the design process, amplitude equations are used to predict their gain, operation frequency, and bandwidth. However, usual amplitude equations do not take into account the real and imaginary parts of the dispersion and characteristic impedance that results from the use of Floquet lines, hindering reliable design. In order to overcome this limitation, we have used the multiple-scale method to include those effects. We demonstrate that complex dispersion and characteristic impedance have a stark effect on the transmission line's gain, even suppressing it completely in certain cases. The equations presented here can, thus, guide to a better design and understanding of the properties of this kind of amplifier.

Index Terms—Four-wave-mixing (FWM), gain, nonlinear physics, parametric amplification, superconductor.

I. INTRODUCTION

ACHIEVING larger bandwidths at the RF and IF bands and improving receiver sensitivity are major challenges for future millimeter and submillimeter heterodyne observations [1]. As part of this effort, extensive work is being done in

Manuscript received 2 October 2022; revised 3 January 2023; accepted 26 January 2023. Date of publication 9 February 2023; date of current version 23 February 2023. This work was supported by ANID under Grant Fondecyt 1180700, Grant Basal ACE210002, and Grant FB210003. The work of Daniel Valenzuela was supported under Grant DOCTORADO BECAS CHILE 2020—21200705. The work of Ricardo Finger was supported under Grant FONDECYT1221662 and Grant FONDEFID211-10359. (Corresponding author: Fausto Patricio Mena.)

Javier Carrasco is with the Electrical Engineering Department and the Department of Physics, Faculty of Physical and Mathematical Sciences, University of Chile, Santiago 8320000, Chile.

Daniel Valenzuela is with the Electrical Engineering Department, Faculty of Physical and Mathematical Sciences, University of Chile, Santiago 8320000, Chile.

Claudio Falcón is with the Department of Physics, Faculty of Physical and Mathematical Sciences, University of Chile, Santiago 8320000, Chile.

Ricardo Finger is with the Department of Astronomy, Faculty of Physical and Mathematical Sciences, University of Chile, Santiago 8320000, Chile.

Fausto Patricio Mena is with the National Radio Astronomy Observatory, Charlottesville, VA 22903 USA (e-mail: pmena@nrao.edu).

Color versions of one or more figures in this article are available at <https://doi.org/10.1109/TASC.2023.3243464>.

Digital Object Identifier 10.1109/TASC.2023.3243464

order to improve the performance of superconductor-insulator-superconductor (SIS) mixers [2] and HEMT amplifiers [3], the key components of current state-of-the-art receivers. However, on the one hand, it is not clear if HEMT amplifiers can be further improved notwithstanding the extensive work made in understanding the reasons that limit noise temperature and operational bandwidth [4], [5], [6]. On the other hand, even if SIS mixers are improved, connecting them to HEMT amplifiers will necessarily limit their performance [7], [8]. Recently, a promising superconducting technology that could overcome these problems has emerged [9]. It uses the kinetic inductance (KI) of superconductors [10], [11] to produce parametric amplification in a long transmission line (TL). Devices working with this principle are dubbed traveling-wave kinetic-inductance parametric amplifiers (TKIPAs) [9], [12], [13], [14], [15], [16].

The KI, originated by the inertia of Cooper pairs [10] in superconductors, modifies the wave equation on the TL by adding nonlinearities, which allow the mixing of wave amplitudes when more than one monochromatic wave are injected [17]. Hence, it is possible to amplify the input signal if other signals, called pumps, are simultaneously injected. Nonetheless, more signals, including undesired harmonics, are also generated, compromising the amplification process. Eom et al. [9] solved this problem by implementing a suitable Floquet TL, also known as *dispersion-engineered TL*, conformed by a periodically repeating unit cell that creates stopbands and, thus, avoids the propagation of the main undesired harmonics of the pump signal. Such a solution, however, translates into a TL with more intricate properties, namely a complex dispersion and characteristic impedance, i.e., with real and imaginary parts, that, moreover, have strong frequency dependencies, particularly close to the stopbands.

In order to design TKIPAs, a nonlinear wave equation must be solved. This is usually done by approximating the process of amplitude gain as a dynamical evolution occurring at a much larger length scale than the wavelength of the involved signals. Within this approximation, but without taking into account the complex nature of the Floquet TL, a set of nonlinear amplitude equations can be obtained [18], [19]. In order to account for losses, an attempt to introduce a complex propagation constant in this approximation has been reported [13] but lacks justification when dealing with the wave behavior near stopbands.

We have included the complex nature of the Floquet TL into the amplitude equations by formally solving the nonlinear wave equation via a multiple-scale method, widely used in nonlinear physics and especially useful in traveling-wave equations [19], [20], [21]. We demonstrate that the use of this type of line has a profound effect on the attainable gain, in particular when the pump signal is close to a stopband. Depending on the specific properties of the used Floquet TL and the amplitude and frequency of the pump signal, our equations depart notably from the predictions given by the traditional amplitude equations.

II. AMPLITUDE EQUATIONS WITH COMPLEX CHARACTERISTIC IMPEDANCE AND DISPERSION

In a TL, the electric current $I = I(z, t)$ and voltage $V = V(z, t)$ dynamics are given by the *telegraph equations*

$$\frac{\partial V}{\partial z} = -L \frac{\partial I}{\partial t} - RI \quad (1a)$$

$$\frac{\partial I}{\partial z} = -C \frac{\partial V}{\partial t} - GV \quad (1b)$$

where z is the position along the TL and t is the time. Here, R is the resistance per unit length due to losses in the conductors, C is the capacitance per unit length due to the close proximity between conductors, G is the conductance per unit length due to losses in the dielectric material between conductors, and L is the total self-inductance per unit length between the conductors [22]. However, for TLs made out of superconductors, the inductance per unit length is a function of the current and can be modeled as

$$L = L_0 \left(1 + \alpha_* \frac{I^2}{I_*^2} \right) \quad (2)$$

where L_0 is the total inductance per unit length of the TL at null electric current, α_* is the ratio of KI to total inductance, and I_* is a parameter comparable to the critical current I_c [9] (which is in the order of a few milliamperes for realizable devices). Importantly, $I_* = I_c' / \sqrt{\alpha_*}$ determines the strength of the nonlinear effect [9], [17].

Expression (2) comes from the fact that the current has a cubic dependence on the velocity of Cooper pairs [23], [24]. It is valid at temperatures $T \ll T_c$ [24], where T_c is the critical temperature of the superconductor, commonly of the order of a few kelvins [11].

From (1) and (2), a nonlinear wave equation for the current can be derived

$$\begin{aligned} \left(\frac{\partial^2}{\partial z^2} - CL_0 \frac{\partial^2}{\partial t^2} - (CR + GL_0) \frac{\partial}{\partial t} - RG \right) I \\ = \frac{L_0}{3I_*^2} \left(G \frac{\partial}{\partial t} + C \frac{\partial^2}{\partial t^2} \right) I^3. \end{aligned} \quad (3)$$

It can be compactly rewritten as

$$\mathcal{L}I = \mathcal{N}I^3 \quad (4)$$

where \mathcal{L} and \mathcal{N} are, respectively, the differential operators acting on the linear and nonlinear parts of the equation. The equation $\mathcal{L}I = 0$ corresponds to the well-known linear wave equation

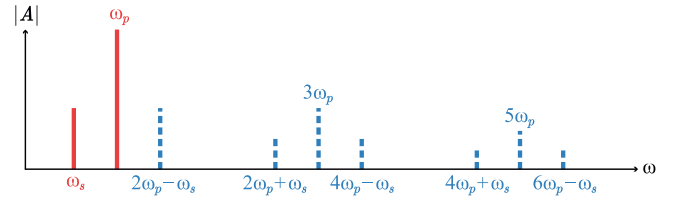


Fig. 1. Fourier spectrum of the main signals relevant in the FWM process [17]. This diagram shows the physically injected signals (solid red), and the signals that are generated in the FWM process (dashed blue). From the latter, the idler with angular frequency $\omega_i \equiv 2\omega_p - \omega_s$, and the third harmonic of the pump with angular frequency $3\omega_p$, are the most relevant. Many more signals appear at higher frequencies, but they are less relevant because they have much smaller amplitudes.

whose general solution, for waves traveling along the TL in the $+z$ direction, is

$$I_{\text{linear}} = \frac{1}{2} \sum_n (A_n e^{j\omega_n t - \gamma_n z} + \text{c.c.}) \quad (5)$$

where “c.c.” stands for “complex conjugate,” $\omega_n \equiv 2\pi\nu_n$ is the angular frequency of the n th tone of I , and γ_n are the propagation constants that fulfill the dispersion relation

$$\gamma_n^2 + CL_0\omega_n^2 - j\omega_n(CR + GL_0) - RG = 0. \quad (6)$$

The solution to $\mathcal{L}I = 0$ can be obtained independently at each frequency. However, if $\alpha_* \neq 0$ (i.e. $\mathcal{N} \neq 0$), the term I^3 allows for interaction between frequencies that, under the correct conditions, can produce amplification of a target frequency signal. The level of amplification depends on a specific parameter, the *pump* signal, which is an injected monochromatic wave used as a source of energy in the process. This is known as *parametric amplification*. Moreover, the cubic nonlinearity means that this is a four-wave-mixing (FWM) process. In consequence, the energy transfer occurs fundamentally by the exchange of pairs of photons, rather than single ones [18]. Therefore, in order to transfer energy from the pump to the signal, an additional monochromatic wave is required, called *idler*, which also receives energy from the pump. The idler is naturally generated in the FWM process together with harmonics and sidebands [17] as depicted in Fig. 1.

A. Multiple-Scale Method

We tackle the problem of solving the nonlinear current (3) using a *multiple-scale method* by considering the nonlinear term $\mathcal{N}I^3$ as a perturbation to the linear wave dynamics $\mathcal{L}I = 0$, which evolves at a different rate or scale [19], [25].

The method is applied to (4) rewritten in terms of $\tilde{I} \equiv I/I_*$. Since $|I| < I_c$ and $I_* \geq I_c$, then $|\tilde{I}| \equiv |I/I_*| < 1$, and it follows that $|\tilde{I}|^3 < |\tilde{I}|$. In consequence, the nonlinear terms can be considered perturbations to the linear equation of the current, acting at scales in z larger than the evolution of the linear equation. The typical spatial scale of the linear part of (4) is the wavelength $2\pi/\beta_n$, where $\beta_n \equiv \text{Im}\{\gamma_n\}$ is the wavenumber, whereas the (nonlinear) typical length scale of the envelope A_n is much larger, as it will be clear later in Section II-B. This information is considered by giving the amplitudes A_n in (5)

dependence on z but only at large scales. Then, to solve at first order, only the dominant z -scale affecting A_n is considered, giving a new wave equation, balanced at first order. The solution to this equation must not contain singular terms, the condition that results in a set of amplitude equations.

We focus on a zone close to the stopbands in Floquet TLs, commonly used to implement amplifiers using this principle [9], [17]. The set of amplitude equations displays solutions that depend on the specific TL used to transport the signals. In particular, we obtain a new model valid in a frequency zone where $CR\omega\tilde{I}$, $GL_0\omega\tilde{I}$, $RG\tilde{I}$, and $CL_0\tilde{I}^3\omega^2/3$ are of around the same order of magnitude because $\tilde{I}^2 \approx \frac{3\tilde{G}}{C\omega}$. Additionally, in the zone of interest, these terms are small enough to be considered first-order perturbations of the $(\gamma^2 + \omega^2 CL_0)\tilde{I} = 0$ equation. Since this zone happens to be near the stopbands in our Floquet TLs, we call our new model near-stopband complex transmission line (NS-CTL).

In order to exemplify the results obtained within this model, we present the case $\tilde{I} = 0.2$, which is a reasonable value of operation and permits comparison with state-of-the-art devices [9], [12], [13], [15], [17]. A thorough study on the effect of varying \tilde{I} , modifying the validity zone will be presented elsewhere.

B. Solution to the Nonlinear Wave Equation

After balancing (3) at first order in the frequency zone of interest, i.e., near the stopbands, we derive the NS-CTL model

$$\left(\frac{\partial^2}{\partial z^2} - CL_0\frac{\partial^2}{\partial t^2}\right)\tilde{I} = \epsilon RG\tilde{I} + \epsilon(CR + GL_0)\frac{\partial}{\partial t}\tilde{I} + \epsilon\left(\frac{L_0C}{3}\frac{\partial^2}{\partial t^2}\right)\tilde{I}^3. \quad (7)$$

This equation can be compactly expressed as

$$\mathcal{L}^{(0)}\tilde{I} = \epsilon\left(\mathcal{L}^{(1)}\tilde{I} + \mathcal{N}^{(1)}\tilde{I}^3\right) \quad (8)$$

where the positive number $\epsilon \ll 1$ is explicitly written to identify the perturbative first-order terms. $\mathcal{L}^{(0)}$ is the operator acting on the unperturbed linear equation while $\mathcal{L}^{(1)}$, and $\mathcal{N}^{(1)}$ are the operators acting as first-order perturbations on the linear and nonlinear parts of the equation, respectively.

Very far from the stopbands in a Floquet TL, the right-hand side of (8) reduces to $\epsilon\mathcal{N}^{(1)}\tilde{I}^3$ because the RG , CR , and GL_0 quantities are too small in those cases, making the term $\mathcal{L}^{(1)}\tilde{I}$ to act at orders smaller than ϵ . However, as we get closer to the stopbands, RG , CR , and GL_0 increase in magnitude, and the term $\mathcal{L}^{(1)}\tilde{I}$ must be included as done in (8). We operate our TKIPA in the frequency zone where this is justified.

Within the NS-CTL model, we apply the multiple-scale method using the zeroth-order solution to (8), i.e., the solution to $\mathcal{L}^{(0)}\tilde{I}^{(0)} = 0$, given by

$$\tilde{I}^{(0)} = \frac{1}{2} \sum_n^N \left(A_n(z_1) e^{j(\omega_n t - \beta_n z)} + \text{c.c.} \right) \quad (9)$$

where, in contrast to (5), A_n now includes a dependence on $z_1 = \epsilon z$, separating it from other scales of z in concordance

with the explanation given in Section II-A. More details of the derivation can be found in [26].

After applying the multiple-scale method using (9) in (8), we obtain the *amplitude equation* for the m th signal

$$\frac{\partial A_m}{\partial z} = jg_m A_m - 2\alpha_m A_m + \frac{jf_m e^{j\beta_m z}}{3 \cdot 8 \cdot I_*^2} \left\langle e^{j\omega_m t} \left| \left(\sum_n^N A_n e^{j(\omega_n t - \beta_n z)} + \text{c.c.} \right)^3 \right. \right\rangle \quad (10)$$

where

$$f_m = \frac{1}{2\beta_m} \left(\alpha_m^2 - \beta_m^2 - \frac{|\gamma_m|^2}{|\eta_m|^2} (r_m^2 - x_m^2) \right) \quad (11)$$

$$g_m = \frac{\alpha_m^2 r_m^2 - \beta_m^2 x_m^2}{\beta_m (r_m^2 + x_m^2)} \quad (12)$$

and

$$\gamma_m = \sqrt{(R_m + j\omega_m L_{0,m})(G_m + j\omega_m C_m)} \quad (13)$$

$$\eta_m = \sqrt{\frac{R_m + j\omega_m L_{0,m}}{G_m + j\omega_m C_m}}. \quad (14)$$

In Floquet TLs the propagation constant $\gamma_m \equiv \alpha_m + j\beta_m$ and the characteristic impedance $\eta_m \equiv r_m + jx_m$ are strongly dependent on the frequency in the zone of interest and have non-negligible real and imaginary parts. We have used the Hermitian inner product defined by

$$\langle a(t) | b(t) \rangle \equiv \frac{1}{2\pi} \int_0^{2\pi} a^*(t) b(t) dt \quad (15)$$

for any couple of time-dependent 2π -periodic complex-valued continuous functions $a(t)$, $b(t)$ as a projector, which allows us to quantify the contribution of one wave to another.

From (10), we observe the two terms contributing to the oscillatory part of the solution for $A_m(z)$ scale in space as $|2\pi/g_m|$ and $|2\pi \cdot 3 \cdot 8/f_m|$, respectively. Therefore, in frequency zones where $\alpha_m \ll \beta_m$ and $|x_m| \ll r_m$, the minimum spatial scale of $A_m(z)$ is given by $|2\pi \cdot 3 \cdot 8/f_m| \approx 2\pi \cdot 24/\beta_m$. This scale is 24 times larger than the wavelength $2\pi/\beta_m$, justifying the use of the multiple-scale method. The exact scale is $\min\{|2\pi/g_m|, |2\pi \cdot 24/f_m|\}$, which varies with the frequency. The scale given by π/α_m is just the decay in z of the amplitudes due to losses, which is much larger than all other scales since $\alpha_m \ll \beta_m$ for all frequencies outside stopbands.

The lossless transmission line (LTL) model used in the literature [9] corresponds to the NS-CTL model but changes the value of the TL parameters $(R_m, G_m, C_m, L_{0,m})$ for ones that neglect $x_m \equiv \text{Im}\{\eta_m\}$ and $\alpha_m \equiv \text{Re}\{\gamma_m\}$. The NS-CTL model reduces to the LTL model in the limiting case of $x_m = \alpha_m = 0$, because then, $R_m G_m = C_m R_m + G_m L_{0,m} = 0$. This makes $g_m = 0$ and $f_m = -\beta_m$, which do not hold for frequencies near the stopbands.

To make the amplitude equations (10) explicit, we need to set the number of waves, N . The signal (s), pump (p), and idler (i)

waves are the minimum required to describe the FWM dynamics and obtain parametric amplification.

C. Signal, Pump, and Idler Interaction ($s-p-i$)

By setting $N = 3$ in the amplitude equations (10) with $n, m = s, p, i$, we obtain a set of three amplitude equations

$$\frac{\partial A_s}{\partial z} = jg_s A_s - 2\alpha_s A_s + j \frac{f_s}{8I_*^2} \times [A_s(|A_s|^2 + 2|A_i|^2 + 2|A_p|^2) + A_i^* A_p^2 e^{j\Delta\beta z}] \quad (16a)$$

$$\frac{\partial A_i}{\partial z} = jg_i A_i - 2\alpha_i A_i + j \frac{f_i}{8I_*^2} \times [A_i(2|A_s|^2 + |A_i|^2 + 2|A_p|^2) + A_s^* A_p^2 e^{j\Delta\beta z}] \quad (16b)$$

$$\frac{\partial A_p}{\partial z} = jg_p A_p - 2\alpha_p A_p + j \frac{f_p}{8I_*^2} \times [A_p(2|A_s|^2 + 2|A_i|^2 + |A_p|^2) + 2A_p^* A_s A_i e^{-j\Delta\beta z}] \quad (16c)$$

where $\Delta\beta \equiv \beta_s + \beta_i - 2\beta_p$.

Interestingly, by writing $A_m \equiv |A_m| e^{j\phi_m}$, the evolution of the modules of the amplitudes can be found as

$$\frac{\partial |A_s|}{\partial z} = -2\alpha_s |A_s| - \frac{f_s}{8I_*^2} |A_i| |A_p|^2 \sin \Theta(z) \quad (17a)$$

$$\frac{\partial |A_i|}{\partial z} = -2\alpha_i |A_i| - \frac{f_i}{8I_*^2} |A_s| |A_p|^2 \sin \Theta(z) \quad (17b)$$

$$\frac{\partial |A_p|}{\partial z} = -2\alpha_p |A_p| + 2 \frac{f_p}{8I_*^2} |A_s| |A_i| |A_p| \sin \Theta(z) \quad (17c)$$

$$\begin{aligned} \frac{\partial \Theta}{\partial z} &= \Delta\beta - \Delta g + \frac{1}{8I_*^2} \left[|A_s|^2 (f_s - 2\Delta f) \right. \\ &\quad \left. + |A_i|^2 (f_i - 2\Delta f) - 2|A_p|^2 (f_p + \Delta f) + \cos \Theta(z) \right. \\ &\quad \left. \times \left(4|A_s| |A_i| f_p - \frac{|A_i| |A_p|^2}{|A_s|} f_s - \frac{|A_s| |A_p|^2}{|A_i|} f_i \right) \right] \quad (17d) \end{aligned}$$

where $\Theta(z) \equiv \Delta\beta z - \Delta\phi(z)$, $\Delta\phi(z) \equiv \phi_s + \phi_i - 2\phi_p$, $\Delta g \equiv g_s + g_i - 2g_p$, and $\Delta f \equiv f_s + f_i - 2f_p$. The phase $\Theta(z)$ is the *total phase mismatch* that consists of a *linear*, $\Delta\beta z$, and a *nonlinear phase mismatch*, $\Delta\phi(z)$. The phase mismatch is relevant because, depending on its value, the transfer of energy flows from the pump toward the signal and idler waves or viceversa [27]. Since $f_m < 0$, the former occurs for $\Theta \in (0, \pi)$, and the latter for $\Theta \in (-\pi, 0)$. Moreover, in the very special cases of $\Theta = 0, \pm\pi$, no transfer of energy happens between the signals. Therefore, thanks to the existence of the phase mismatch, these amplitude equations predict the possibility of amplifying the target signal. Furthermore, the ideal situation occurs when $\Theta = \frac{\pi}{2}$, maximizing the transfer rate of energy toward the target signal.

D. Including Pumps' Third Harmonic ($s-p-i-3p$)

The $s-p-i$ case can be improved by including the wave of the third harmonic of the pump ($3p$). For doing so, we set $N = 4$, implying that this time we get a set of four amplitude equations

$$\begin{aligned} \frac{\partial A_s}{\partial z} &= jg_s A_s - 2\alpha_s A_s + j \frac{f_s}{8I_*^2} \\ &\quad \times [A_s(|A_s|^2 + 2|A_i|^2 + 2|A_p|^2 + 2|A_{3p}|^2) \\ &\quad \quad + A_i^* A_p^2 e^{j\Delta\beta z} + 2A_i^* A_p^* A_{3p} e^{j\Delta\beta_2 z}] \quad (18a) \end{aligned}$$

$$\begin{aligned} \frac{\partial A_i}{\partial z} &= jg_i A_i - 2\alpha_i A_i + j \frac{f_i}{8I_*^2} \\ &\quad \times [A_i(2|A_s|^2 + |A_i|^2 + 2|A_p|^2 + 2|A_{3p}|^2) \\ &\quad \quad + A_s^* A_p^2 e^{j\Delta\beta z} + 2A_s^* A_p^* A_{3p} e^{j\Delta\beta_2 z}] \quad (18b) \end{aligned}$$

$$\begin{aligned} \frac{\partial A_p}{\partial z} &= jg_p A_p - 2\alpha_p A_p + j \frac{f_p}{8I_*^2} \\ &\quad \times [A_p(2|A_s|^2 + 2|A_i|^2 + |A_p|^2 + 2|A_{3p}|^2) \\ &\quad \quad + 2A_p^* A_s A_i e^{-j\Delta\beta z} + 2A_s^* A_i^* A_{3p} e^{j\Delta\beta_2 z} \\ &\quad \quad + A_{3p} (A_p^*)^2 e^{j\Delta\beta_3 z}] \quad (18c) \end{aligned}$$

$$\begin{aligned} \frac{\partial A_{3p}}{\partial z} &= jg_{3p} A_{3p} - 2\alpha_{3p} A_{3p} + j \frac{f_{3p}}{8I_*^2} \\ &\quad \times [A_{3p}(2|A_s|^2 + 2|A_i|^2 + 2|A_p|^2 + 2|A_{3p}|^2) \\ &\quad \quad + \frac{1}{3} A_p^3 e^{-j\Delta\beta_3 z} + 2A_s A_i A_p e^{-j\Delta\beta_2 z}] \quad (18d) \end{aligned}$$

where $\Delta\beta_2 \equiv \beta_s + \beta_i + \beta_p - \beta_{3p}$, and $\Delta\beta_3 \equiv 3\beta_p - \beta_{3p}$.

The presence of the third harmonic of the pump can greatly reduce the signal gain in the FWM process of the TKIPA. To properly account for this effect, the $3p$ wave must be taken into consideration, requiring the use of the amplitude equations (18). Nevertheless, we know from the linear wave solution in TLs, i.e., (5) and (6), that the $3p$ wave is suppressed if its frequency is inside a stopband. Therefore, we expect the same to happen with the set of amplitude equations (18), allowing us to simplify it to (16). In Section IV, we simulate both sets of amplitude equations to verify that this is the case.

III. DIFFERENCES BETWEEN LTL AND NS-CTL MODELS

The amplitude equations of the LTL model can be obtained for the $s-p-i$ and $s-p-i-3p$ cases by setting $\alpha_m = x_m = 0$, which gives $g_m = \alpha_m = 0$ and $f_m = -\beta_m$ in (16)–(18) for all $m = s, p, i, 3p$. This sets two important differences between the models, one related to the factor f_m and other to g_m .

In the NS-CTL model, the relevant constant factor for amplification is f_m . This fact can be seen from (17) by noticing that the coupling terms, allowing energy transfer, are proportional to f_m . Hence, in order to obtain gain of the target signal, the larger it can be, the better.

In the LTL model, instead, the relevant constant factor for amplification reduces to $-\beta_m$, obtained neglecting the effect of α_m and x_m in (11). Therefore, the LTL model has less degrees of

TABLE I
PARAMETERS OF THE MATERIALS MAKING UP THE CPW LINE

Parameter (Unit)	NbTiN		Si	
	T_c (K)	ρ_N ($\mu\Omega \cdot \text{cm}$)	ϵ_r	$\tan \delta$
Value	14.7	100	11.44	0
Reference	[31], [32]	[9]	[33]	–

freedom to optimize this factor. Nonetheless, $f_m \approx -\beta_m$ is an acceptable approximation for frequencies near stopbands where the NS-CTL model is valid.

On the other hand, the term g_m in the NS-CTL model affects the equation for $|A_m|$ through the phase mismatch $\Theta(z)$. This effect can be concluded by noticing the presence of the Δg term in (17d). Therefore, g_m affects (17 a–c) through the $\sin(\Theta)$ term, which multiplies the f_m factor. Consequently, g_m can produce a big impact in the amplification process by increasing or reducing the rate of energy transfer from the pump to the signal and idler. This is the most important effect that is absent in the LTL model, where $g_m = 0$, as it is the only difference affecting directly the nonlinear dynamics and, therefore, amplification. Hence, if there is any relevant difference in the simulations between the LTL and NS-CTL models, it is due to the effect of g_m on the phase mismatch $\Theta(z)$.

IV. RESULTS AND DISCUSSION

We have designed and simulated a Floquet coplanar waveguide (CPW) TL made out of a central TL, with propagation constant $\gamma_0 \equiv \alpha_0 + j\beta_0$ and characteristic impedance $\eta_0 \equiv r_0 + jx_0$, that contains small sections of different strip width that are periodically repeated. The complete Floquet TL has an effective propagation constant $\gamma \equiv \alpha + j\beta \neq \gamma_0$ and effective characteristic impedance $\eta \equiv r + jx \neq \eta_0$. This line is designed to have frequency stopbands, defined by $\delta\alpha \equiv \alpha - \alpha_0 \neq 0$, and a nonlinear dispersion relation $\beta(\nu)$ near the stopbands, identified by $\delta\beta \equiv \beta - \beta_0 \neq 0$. The latter is very important because it allows us to tune the linear phase mismatch $\Delta\beta z \equiv \beta_s z + \beta_i z - 2\beta_p z$, relevant for the amplification of the target signal, as discussed in Section II-C.

In the simulations presented ahead, we have considered initial pump amplitudes A_p^0 in the order of $0.1I_*$, and a much smaller initial signal amplitude $A_s^0 = 10^{-7}I_*$, resembling the detection of small astronomical signals. The six (12) orders of magnitude that separate the pump and the signal in terms of amplitude (power) are large enough not to reach appreciable pump depletion in the simulations.

A. Design

Our Floquet TL design is shown in Fig. 2, where we have used a CPW geometry. The design parameters are given in Tables I and II. The parameters α_0 and x_0 are negligible compared to $\beta_0/\nu \approx 112 \text{ m}^{-1} \cdot \text{GHz}^{-1}$ and $r_0 \approx 127 \Omega$, respectively. The parameters were calculated for a temperature $T = 4 \text{ K}$. The

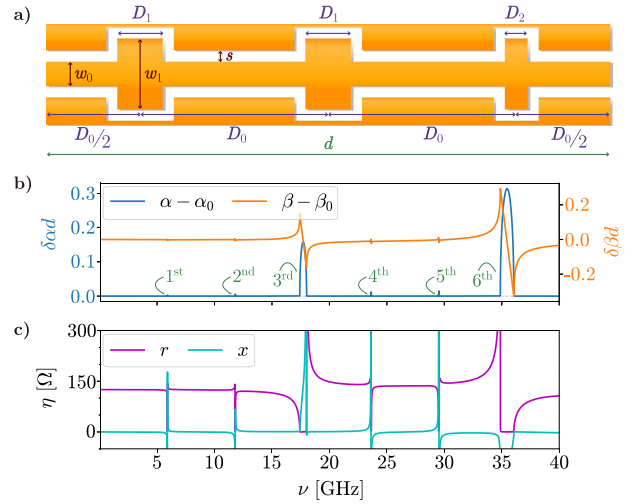


Fig. 2. (a) CPW-based Floquet TL consisting of a central line of width w_0 and dispersive loads of width w_1 , both with the same thickness t . Their values, together with those of the separation s and the lengths D_0, D_1, D_2 , and d , are given in Table II. (b) Dispersion of the designed Floquet TL. Six stopbands are shown and enumerated in green. They are determined by $\delta\alpha \equiv \alpha - \alpha_0 \neq 0$, where the subindex “0” indicates “central line.” Around the stopbands, a steeply changing nonlinear dispersion relation is observed, i.e., $\delta\beta \equiv \beta - \beta_0 \neq 0$. (c) Characteristic impedance of the Floquet TL. It is noticeable that r and x have a strong variation close to the stopbands.

TABLE II
GEOMETRIC PARAMETERS OF THE CPW FLOQUET TL

t (nm)	s (μm)	w_0 (μm)	w_1 (μm)	D_0 (mm)	D_1 (μm)	D_2 (μm)	d (mm)
35	1	1	3.4	1.578	60	50	4.734

superconductor’s conductivity was calculated via the formulation given by Mattis and Bardeen [28], [29]. The superficial impedance and geometric factors of the CPW were calculated using the method described by Zhao et al. [30]. Table I lists the material properties of the dielectric and superconductor making up the designed CPW line.

In our simulations, we have set the operation of the TKIPA with the pump near the second stopband and its third harmonic in the sixth stopband. The relevant quantities at these frequencies are shown in Fig. 3, where the order of magnitude of each of the terms of (3) is plotted as the function of the frequency. Our NS-CTL model is valid in a frequency zone where the terms $CR\omega\tilde{I}$, $GL_0\omega\tilde{I}$, $RG\tilde{I}$, and $CL_0\tilde{I}^3\omega^2/3$ are of around the same order ϵ below the dominant term $(\gamma^2 + \omega^2 CL_0)\tilde{I}$. This happens at frequencies near any of the stopbands, including our choice. We choose the pump frequency ν_p to be in the green dashed regions because then the $3p$ wave falls inside the sixth stopband allowing its suppression.

B. Effect of the Pump’s Third Harmonic

In order to study the effect of the pump’s third harmonic and check the consistency of (16) and (18), we applied them to two different pump frequencies, ν_p . Furthermore, we repeated

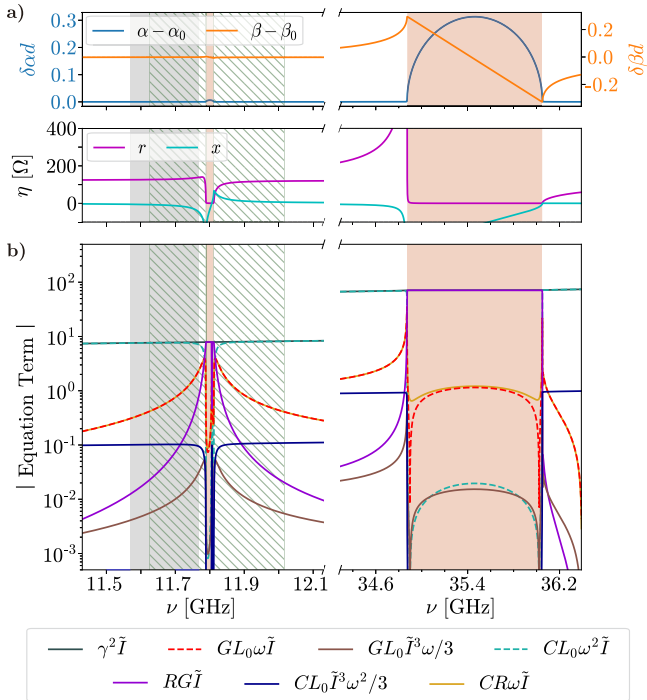


Fig. 3. (a) Dispersion relation and characteristic impedance from Fig. 2 zoomed in around the second (left column) and sixth (right column) stopbands (marked as red zones). (b) Magnitudes of the different terms of (3) for the case $\tilde{I} \equiv I/I_* = 0.2$. The green dashed zones on the left, correspond to frequencies where its third harmonic, 3ν , falls within the stopband shown on the right. The grayed-out region corresponds to the validity zone of the NS-CTL model at frequencies below the second stopband. When $\tilde{I} = 0.2$, this region ranges from 11.57 to 11.77 GHz but decreases at higher values of \tilde{I} .

the simulations using the corresponding approximations for the traditional LTL model.

The first frequency, $\nu_p = 11.33$ GHz, corresponds to a situation where $3\nu_p$ is well outside the sixth stopband. In this case, the $3p$ wave should not be suppressed and all the signal gain should be lost. The situation is well captured by (18), in both the NS-CTL and LTL models, as demonstrated by the left panel of Fig. 4(a). On the contrary, (16) wrongly predicts gain as it does not consider the pump's third harmonic [see right panel of Fig. 4(a)].

In the second situation, $\nu_p = 11.63$ GHz, $3\nu_p$ is well inside the sixth stopband. Here, the $3p$ wave should be suppressed and the TL should produce gain. The situation is now well described by (18) only in the NS-CTL model [left panel of Fig. 4(b)]. The LTL model cannot predict gain because the assumption $\alpha = 0$ impedes the detection of stopbands, meaning that the $3p$ wave is not suppressed in this simulation. Importantly now, for the NS-CTL case, (16) and (18) give identical results [both panels of Fig. 4(b)], demonstrating the consistency of the framework used here.

In Fig. 4(b), we also observe that, compared to the LTL model, the NS-CTL model predicts higher signal gain. The reason for this result is that the total phase mismatch $\Theta(z)$ evolves differently in each model. We thoroughly explain this effect in Section IV-D.

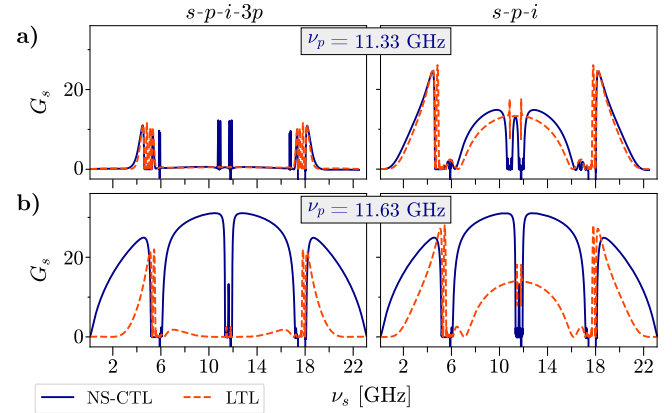


Fig. 4. Gain of the target signal after traveling $z/d = 150$ unit cells through the parametric amplifier. The simulations correspond to two different values of pump frequency ν_p near the second stopband with an initial pump amplitude $A_p^0 = 0.2I_*$. Situations in which the third harmonic $3\nu_p$ does not (a) fall and (b) falls in a stopband are presented. The results show that only if the $3p$ signal is suppressed, it can be correctly disregarded in the NS-CTL model.

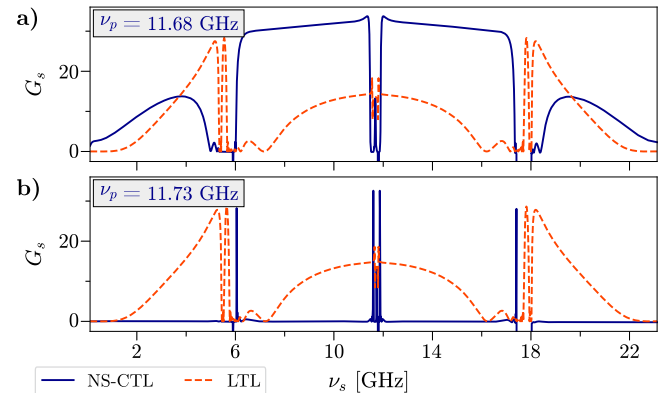


Fig. 5. Parametric gain of the target signal after traveling $z/d = 150$ unit cells. The simulations correspond to two values of ν_p close to the second stopband, suppressing the $3p$ signal. In both cases, an initial pump amplitude $A_p^0 = 0.2I_*$ was used. (a) In the first case, the NS-CTL model predicts an enhancement of the gain of the target signal. (b) When the pump frequency is even closer to the stopband, the loss term $|RG\tilde{I}|$ dominates over the nonlinear one, $|CL_0\tilde{I}^3\omega^2/3|$, resulting in no gain.

C. Effect of the Stopband on the Gain

Now we study the effect of moving ν_p closer to the stopband. With that purpose, we performed two more simulations, one with $\nu_p = 11.68$ GHz [see Fig. 5(a)], and another with $\nu_p = 11.73$ GHz [see Fig. 5(b)]. In both cases, the third harmonic of the pump is being suppressed, so we only show results for the $s-p-i$ case.

By comparing Figs. 5(a) and 4(b), we observe that setting ν_p closer to a stopband results in a larger gain, either using the LTL or the NS-CTL model. Nevertheless, if we keep moving ν_p even closer to the stopband, we predict no gain with the NS-CTL model [see Fig. 5(b)]. This occurs because at frequencies too close to a stopband (like $\nu_p = 11.73$ GHz), the loss term $RG\tilde{I}$ dominates over the nonlinear term, $CL_0\tilde{I}^3\omega^2/3$. Therefore, the nonlinear dynamics responsible for amplification are overcome.

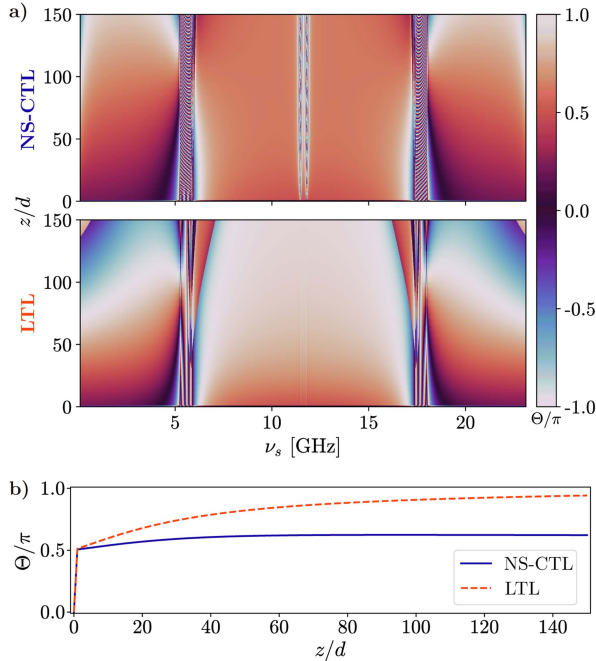


Fig. 6. (a) Color-coded plot of the evolution of the phase mismatch $\Theta(z)$, for the NS-CTL and LTL models, as a function of the signal frequency ν_s . The simulation corresponds to the TKIPA pumped at $\nu_p = 11.63$ GHz. It is observed that $\Theta(z)$ is better stabilized near $\pi/2$ along all the evolution in the NS-CTL model, meaning an energy transfer from the pump to the idler and target signals close to the optimal value along all z . (b) Cut off the $\Theta(z)$ evolution at $\nu_s = 10$ GHz to stress the difference between the two models.

by loss dynamics, resulting in no gain of the target signal. The LTL model does not consider this complexity because it neglects α and x , implying neglecting RG . Consequently, the LTL model still predicts gain at the same frequency.

D. Effect of $\Theta(z)$ on the Gain

As explained in Section III, the main difference between the NS-CTL and LTL models resides in the g_m term that directly modifies the phase mismatch $\Theta(z)$. Therefore, the differences observed between the two models [such as, e.g., in Fig. 4(b)] should be justified by the evolution of $\Theta(z)$ in each case. To illustrate that this is indeed the case, Fig. 6 presents the evolution of $\Theta(z)$ as a function of the signal frequency for $\nu_p = 11.63$ GHz. We see how the NS-CTL model stabilizes $\Theta(z)$ close to its optimal value $\pi/2$ along the whole dynamical evolution (i.e., through z). Instead, in the LTL model, $\Theta(z)$ varies between optimal and counter-optimal values, for a given signal frequency ν_s , which means that at times of the evolution, the energy transfer is mainly going from the signal and idler to the pump, contrary to the desired performance. Consequently, as long as the nonlinear term $|CL_0\tilde{I}^3\omega^2/3|$ is larger than the loss term $|RG\tilde{I}|$, the LTL model does not predict as much gain of the signal as the NS-CTL model, explaining the difference between the models.

E. Effect of the Initial Pump Amplitude on the Gain

We have also explored how G_s changes by varying the magnitude of the initial pump amplitude $|A_p^0|$. To characterize this

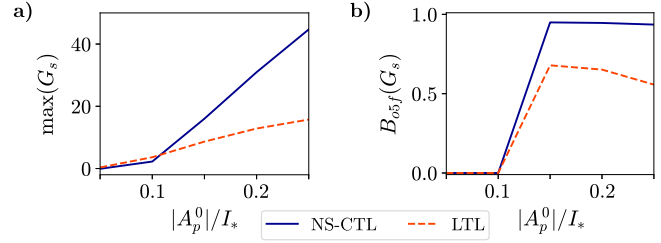


Fig. 7. (a) Maximum gain and (b) over-5dB-fractional bandwidth, B_{o5f} , at $z/d = 150$ and $\nu_p = 11.63$ GHz, for various values of initial pump amplitude A_p^0 . The maximum gain is calculated around the pump frequency, before falling to zero close to 6 and 17 GHz and excluding the center zone where the gain changes curvature.

effect, we have used two figures of merit, maximum gain, and fractional bandwidth for gain over 5 dB (B_{o5f}), plotted in Fig. 7. The span of $|A_p^0|$ corresponds to its largest possible value so that, first, the TKIPA is still operated in the zone where the NS-CTL model is valid and, second, it is reasonably below the critical current. Both LTL and NS-CTL models are presented.

Within the span of initial pump amplitudes used in the simulations, Fig. 7 shows a stark contrast between the LTL and NS-CTL. The latter predicts a larger gain with no evident saturation (panel a) and larger bandwidth (panel b). We attribute this effect to the fact that, for the NS-CTL model, $\Theta(z)$ stabilizes over a wider range of signal frequencies, as shown in Fig. 6.

For larger values of $|A_p^0|$, the maximum gain predicted by the NS-CTL model is expected to, slowly, saturate. However, it must be noted that at such large values, the pump frequency is left outside the validity zone of the model since it depends strongly on the current intensity [26].

The practical result obtained from this analysis is that, if the Floquet TL is designed adequately, the NS-CTL model predicts a better performance than the LTL model if the frequency and amplitude of the pump are chosen correctly to ensure amplification. We believe that previous implementations of the TKIP have not achieved the large gains presented here because, most probably, they are not operating in the correct parameter space. Such space is difficult to accomplish if the validity zone of the NS-CTL model is not carefully considered during the design process. Even in our design, the frequency range where the model is valid while suppressing the pump's third harmonic spans for less than 200 MHz (intersection of gray and dashed green regions in Fig. 3). We are currently working on new designs that substantially increase this frequency range for easier experimental verification.

F. Design Recommendations

From the previous analyses, we are able to give some recommendations for future designs of TKIPAs. First, in order to improve the gain of the target signal, the pump frequency must be in the frequency zone where the NS-CTL model is valid, with the third harmonic of the pump being suppressed by a stopband. Additionally, the order of magnitude of the $RG\tilde{I}$ term must be smaller than the one of the $CL_0\tilde{I}\omega^3/3$ term in the nonlinear wave equation for the electric current. If, furthermore, $\beta(\nu)$ is highly nonlinear around the pump frequency, large

amplification of the target signal is expected. Fulfilling all these design criteria implies selecting appropriately the strength and width of the stopbands.

V. CONCLUSION

We have presented a new set of amplitude equations for TKIPAs operated at pump frequencies near the selected stopband (NS-CTL model). Unlike the model commonly used in the literature (LTL), the effects of complex dispersion and characteristic impedance have not been neglected. We compared the two models performing simulations of a TKIPA made from a CPW Floquet TL. The results showed that the new NS-CTL model could predict either larger or smaller gain than the traditional one (LTL), depending on how close the pump frequency is to the stopband. This effect occurs because one of the new terms added to the amplitude equations is capable of stabilizing the phase mismatch, hence obtaining a larger gain. However, this term can also dominate the dynamics over the nonlinear term responsible for amplification since its magnitude depends on the frequency, quenching the attainable gain. Research to experimentally demonstrate these effects is underway.

REFERENCES

- [1] J. Carpenter, D. Iono, F. Kamper, and A. Wooten, "The ALMA development program: Roadmap to 2030," *Monthly Newslett. Int. URSI Commission J. Radio Astron.*, 2020, p. 1. [Online]. Available: https://www.ursi.org/files/CommissionReports/J_news_2020_01.pdf
- [2] T. Kojima et al., "Demonstration of a wideband submillimeter-wave low-noise receiver with 4-21 GHz IF output digitized by a high-speed 32 GSps ADC," *Astron. Astrophys.*, vol. 640, 2020, Art. no. L9.
- [3] P. Yagoubov et al., "Wideband 67-116 GHz receiver development for ALMA band 2," *Astron. Astrophys.*, vol. 634, 2020, Art. no. A46.
- [4] M. W. Pospieszalski, "On the limits of noise performance of field effect transistors," in *Proc. IEEE MTT-S Int. Microw. Symp.*, 2017, pp. 1953-1956.
- [5] M. W. Pospieszalski, "Extremely low-noise cryogenic amplifiers for radio astronomy: Past, present and future," in *Proc. 22nd Int. Microw. Radar Conf.*, 2018, pp. 1-6.
- [6] A. J. Ardizzi et al., "Self-heating of cryogenic high electron-mobility transistor amplifiers and the limits of microwave noise performance," *J. Appl. Phys.*, vol. 132, no. 8, 2022, Art. no. 084501, doi: [10.1063/5.0103156](https://doi.org/10.1063/5.0103156).
- [7] M. W. Pospieszalski, "On extending the IF bandwidth of ALMA band # 6 SIS mixers," 2020. [Online]. Available: <https://zenodo.org/record/5550951>
- [8] A. R. Kerr et al., "Development of the ALMA Band-3 and Band-6 sideband-separating SIS mixers," *IEEE Trans. THz Sci. Technol.*, vol. 4, no. 2, pp. 201-212, Mar. 2014.
- [9] B. H. Eom et al., "A wideband, low-noise superconducting amplifier with high dynamic range," *Nature Phys.*, vol. 8, pp. 623-627, 2012.
- [10] J. Zmuidzinas, "Superconducting microresonators: Physics and applications," *Annu. Rev. Condens. Matter Phys.*, vol. 3, no. 1, pp. 169-214, 2012, doi: [10.1146/annurev-conmatphys-020911-125022](https://doi.org/10.1146/annurev-conmatphys-020911-125022).
- [11] A. Alexandrov, *Theory of Superconductivity: From Weak to Strong Coupling*. Boca Raton, FL, USA: CRC Press, 2003.
- [12] S. Chaudhuri et al., "Broadband parametric amplifiers based on nonlinear kinetic inductance artificial transmission lines," *Appl. Phys. Lett.*, vol. 110, no. 15, 2017, Art. no. 152601, doi: [10.1063/1.4980102](https://doi.org/10.1063/1.4980102).
- [13] S. Zhao, S. Withington, D. J. Goldie, and C. N. Thomas, "Loss and saturation in superconducting travelling-wave parametric amplifiers," *J. Phys. D: Appl. Phys.*, vol. 52, no. 41, Jul. 2019, Art. no. 415301, doi: [10.1088/2F1361-6463%2F5241415301](https://doi.org/10.1088/2F1361-6463%2F5241415301).
- [14] M. Malnou et al., "Three-wave mixing kinetic inductance traveling-wave amplifier with near-quantum-limited noise performance," *PRX Quantum*, vol. 2, Jan. 2021, Art. no. 010302, doi: [10.1103/PRXQuantum.2.010302](https://doi.org/10.1103/PRXQuantum.2.010302).
- [15] S. Shu et al., "Nonlinearity and wide-band parametric amplification in a (Nb,Ti)N microstrip transmission line," *Phys. Rev. Res.*, vol. 3, Jun. 2021, Art. no. 023184, doi: [10.1103/PhysRevResearch.3.023184](https://doi.org/10.1103/PhysRevResearch.3.023184).
- [16] M. Malnou et al., "Performance of a kinetic inductance traveling-wave parametric amplifier at 4 Kelvin: Toward an alternative to semiconductor amplifiers," *Phys. Rev. Appl.*, vol. 17, no. 4, Apr. 2022, Art. no. 044009, doi: [10.1103/PhysRevApplied.17.044009](https://doi.org/10.1103/PhysRevApplied.17.044009).
- [17] S. Chaudhuri, J. Gao, and K. Irwin, "Simulation and analysis of superconducting traveling-wave parametric amplifiers," *IEEE Trans. Appl. Supercond.*, vol. 25, no. 3, Jun. 2015, Art. no. 1500705.
- [18] P. Powers and J. Haus, *Fundamentals of Nonlinear Opt.* Boca Raton, FL, USA: CRC Press, 2017. [Online]. Available: https://books.google.cl/books?id=m-O_DgAAQBAJ
- [19] J. Moloney and A. Newell, *Nonlinear Opt.* Boca Raton, FL, USA: CRC Press, 2018. [Online]. Available: <https://books.google.cl/books?id=EUpaDwAAQBAJ>
- [20] A. H. Nayfeh and D. T. Mook, "Introduction," *Nonlinear Oscillations*. Hoboken, NJ, USA: Wiley, 1995, ch. 1, pp. 1-38, doi: [10.1002/9783527617586.ch1](https://doi.org/10.1002/9783527617586.ch1).
- [21] A. H. Nayfeh and D. T. Mook, "Parametrically Excited Systems," *Nonlinear Oscillations*. Hoboken, NJ, USA: Wiley, 1995, ch. 5, pp. 258-364. [Online]. Available: <https://onlinelibrary.wiley.com/doi/abs/10.1002/9783527617586.ch5>
- [22] D. M. Pozar, *Microwave Engineering*, 3rd ed. Hoboken, NJ, USA: Wiley, 2012.
- [23] S. Cho, "Temperature and current dependence of inductance in a superconducting meander line," *J. Korean Phys. Soc.*, vol. 31, no. 1, pp. 337-341, Aug. 1997.
- [24] S. Anlage, H. Snortland, and M. Beasley, "A current controlled variable delay superconducting transmission line," *IEEE Trans. Magn.*, vol. 25, no. 2, pp. 1388-1391, Mar. 1989.
- [25] B. Young, S. Fauve, B. E. DeRemer, and S. Meacham, "1991 Summer Study Prog. in Geophysical Fluid Dyn.: Patterns in fluid flow," Woods Hole Oceanographic Inst., Falmouth, MA, USA, Tech Rep. WHOI-92-16, 1991, doi: [10.1575/1912/802](https://doi.org/10.1575/1912/802).
- [26] J. Carrasco, "Parametric amplification of electromagnetic signals with superconducting transmission lines," M.Sc. thesis, Dept. Elect. Eng., Univ. Chile, Santiago, Chile, 2022. [Online]. Available: <https://repositorio.uchile.cl/handle/2250/188228>
- [27] J. Hansryd, P. Andrekson, M. Westlund, J. Li, and P.-O. Hedekvist, "Fiber-based optical parametric amplifiers and their applications," *IEEE J. Sel. Topics Quantum Electron.*, vol. 8, no. 3, pp. 506-520, May/Jun. 2002.
- [28] D. C. Mattis and J. Bardeen, "Theory of the anomalous skin effect in normal and superconducting metals," *Phys. Rev.*, vol. 111, pp. 412-417, Jul. 1958, doi: [10.1103/PhysRev.111.412](https://doi.org/10.1103/PhysRev.111.412).
- [29] S. Zhao, D. J. Goldie, S. Withington, and C. N. Thomas, "Exploring the performance of thin-film superconducting multilayers as kinetic inductance detectors for low-frequency detection," *Supercond. Sci. Technol.*, vol. 31, no. 1, Nov. 2017, Art. no. 015007, doi: [10.1088/1361-6668/aa94b7](https://doi.org/10.1088/1361-6668/aa94b7).
- [30] S. Zhao, S. Withington, D. J. Goldie, and C. N. Thomas, "Electromagnetic models for multilayer superconducting transmission lines," *Supercond. Sci. Technol.*, vol. 31, no. 8, Jul. 2018, Art. no. 085012, doi: [10.1088/1361-6668/aacc53](https://doi.org/10.1088/1361-6668/aacc53).
- [31] L. Jiang et al., "Development of THz waveguide NbTiN HEB mixers," *IEEE Trans. Appl. Supercond.*, vol. 19, no. 3, pp. 301-304, Jun. 2009.
- [32] D. J. Thoen, B. G. C. Bos, E. A. F. Haalebos, T. M. Klapwijk, J. J. A. Baselmans, and A. Endo, "Superconducting NbTiN thin films with highly uniform properties over a \emptyset 100 mm wafer," *IEEE Trans. Appl. Supercond.*, vol. 27, no. 4, Jun. 2017, Art. no. 1500505.
- [33] J. Lamb, "Miscellaneous data on materials for millimetre and submillimetre optics," *Int. J. Infrared Millimeter Waves*, vol. 17, pp. 1997-2034, 1996.

Javier Carrasco received the bachelor's degree in electrical engineering in 2017 and the master's degree in physics in 2021 and the bachelor's and master's degrees in electrical engineering in 2018 and 2022, respectively, from Universidad de Chile, Santiago, Chile. He has been working toward the Ph.D. degree in quantum memories and networks with the Group of Applied Physics (GAP), University of Geneva, Switzerland, since February 1, 2023. His physics thesis involved studying quantum batteries analytically and performing simulations of light-matter interaction systems. His electrical engineering thesis involved developing a new framework to design superconducting kinetic-inductance parametric amplifiers, predicting novel behavior.

His research interests include developing new technologies using electro-dynamics and quantum mechanics, currently focusing on studying and developing quantum memories and single-photon emitters using rare Earth-ion doped crystals for applications in quantum networks.

Daniel Valenzuela is currently working toward the Ph.D. degree in study and development of traveling-wave kinetic inductance parametric amplifiers with the Department of Electrical Engineering, Universidad de Chile, Santiago, Chile. His dissertation consists of the design and characterization of parametric amplifiers using artificial CPW lines and comparison with other transmission lines.

He has worked with the Millimeter Wave Laboratory, Universidad de Chile, in superconducting materials, microwave measurements, high-frequency circuits, and microwave simulation software. He has worked with the Space and Planetary Exploration Laboratory in the camera software for SUCHAI I and the communication system for SUCHAI II.

Claudio Falcón received the bachelor's and master's degrees in physics from Universidad de Chile, Santiago, Chile, in 2004, and 2005, respectively, and the Ph.D. degree in out-of-equilibrium statistical mechanics from Université Paris VI Pierre et Marie Curie, now Paris Sorbonne University, Paris, France, in 2008.

He is currently an Associate Professor with Physics Department, Faculty of Physical and Mathematical Sciences, Universidad de Chile. He joined the Laboratory of Matter Out-Of-Equilibrium, Physics Department, Faculty of Physical and Mathematical Sciences, Universidad de Chile, in 2009. His research interests include experimental, theoretical, and numerical study of nonlinear and complex systems, with a focus on wave structure interactions for the development of mechanical metamaterials and nonlinear wave control.

Ricardo Finger received the Ph.D. degree in electrical engineering and a double major degree in engineering and physics from Universidad de Chile, Santiago, Chile, in 2013, and 2004, respectively.

He is currently an Associate Professor with the Department of Astronomy, Universidad de Chile. He develops antennas and receivers from millimeter to centimeter wavelengths and FPGA-based digital signal processors for radio astronomy. He has worked in USA, Sweden, U.K., and with the ALMA Observatory in Chile, in the design, assembly, integration, and verification of cryogenic receivers. He leads the technology transfer effort of the Center for Astrophysics and Associated Technologies (CATA), where he develops microwave-phased arrays and sensor networks for industrial applications.

F. Patricio Mena received the B.S. degree in physics from Escuela Politécnica Nacional, Quito, Ecuador, and the M.S. and Ph.D. degrees in physics from the University of Groningen, Groningen, The Netherlands, in 1994, 2000, and 2004, respectively.

He is currently an Associate Scientist/Research Engineer with the National Radio Astronomy Observatory, Charlottesville, VA, USA. In 2004, he joined the Netherlands Institute for Space Research (SRON), Groningen, The Netherlands, as an Instrument Scientist with Low Energy Division. From 2008 to 2020, he was with Universidad de Chile, where he cofounded the Radio Astronomical Instrumentation Group and the Millimeter/Submillimeter Wave Laboratory. His research interests include the design, fabrication, and characterization of components and systems used in radio astronomical instrumentation.